

Rational design of complex phenotype via network models

Marcio Gameiro^{*,a,b}, Tomáš Gedeon^{†,c}, Shane Kepley^{‡,a}, and Konstantin Mischaikow^{§,a}

^aDepartment of Mathematics, Rutgers, The State University of New Jersey, Piscataway, NJ, 08854

^bInstituto de Ciências Matemáticas e de Computação, Universidade de São Paulo, Caixa Postal 668, 13560-970, São Carlos, SP, Brazil

^cDepartment of Mathematical Sciences, Montana State University, Bozeman, MT, 59715

May 30, 2022

Abstract

We demonstrate a modeling and computational framework that allows for rapid screening of thousands of potential network designs for particular dynamic behavior. To illustrate this capability we consider the problem of hysteresis, a prerequisite for construction of robust bistable switches and hence a cornerstone for construction of more complex synthetic circuits. We evaluate and rank all three node networks according to their ability to robustly exhibit hysteresis. Focusing on the highest ranked networks, we demonstrate how additional robustness and design constraints can be applied. We compare our results to more traditional methods based on specific parameterization of ordinary differential equation models and demonstrate a strong qualitative match at a small fraction of the computational cost.

Keywords: Bistable switch | Synthetic biology | 3-node networks | DSGRN.

Significance Statement: A major challenge in the domains of systems and synthetic biology is an inability to efficiently predict function(s) of complex networks. This work demonstrates a modeling and computational framework that allows for a mathematically justifiable rigorous screening of thousands of potential network designs for a desired dynamic behavior. Although the framework allows for the identification of a wide variety of dynamical behavior, we screen all 3-node genetic networks and rank them based on their ability to act as an inducible bistable switch. Our results are summarized in a searchable database of designs that can be used by synthetic biologists to construct robust switches. The ability to quickly screen thousands of designs significantly reduces the set of viable designs and allows designers to focus their experimental and more traditional modeling tools on this much smaller set.

^{*}gameiro@math.rutgers.edu

[†]gedeon@math.montana.edu

[‡]sk2011@math.rutgers.edu

[§]mischaik@math.rutgers.edu

1 Introduction

Ever since the dawn of cellular biology, the central analogy that we employ to describe cells is that of miniature machines that transform the information about its environment to appropriate responses. The responses take the form of increased or decreased gene expression, protein activation or deactivation, or regulation of transport between cellular compartments and exterior of the cell. There is only a short step from viewing cells as little machines to the desire of controlling them, repairing them, and then building new cellular functions. This is the starting point of synthetic biology [4, 20, 1, 18]; for recent review of progress and challenges see [3]. The success of engineered mechanical or electronic systems, crucially depends on (i) modularity of their designs and (ii) ability to model complicated assemblies of parts before they are built. In synthetic biology both of these steps present significant challenges. The focus of this contribution is on a novel mathematical approach to addressing the second challenge.

The strength of our approach that we call Dynamic Signatures Generated by Regulatory Networks (DSGRN) is that we are agnostic to the specific biochemical or biophysical design of the elements of the circuits that we analyze. The input consists of a mathematical abstraction of a gene regulatory network, e.g. Figure 1(a), that consists of nodes and annotated directed edges indicating activation or repression. The user is required to provide a means of scoring the behavior of the network from the information about dynamics that is computed by DSGRN. The DSGRN software [5] then allows a ranking of the networks in question based on this score.

To demonstrate the applicability of DSGRN we focus on the question of design of a hysteretic switch. There are three reasons that make this a natural choice. First, it is conceptually simple. The same ideas can be applied to the design or analysis of more complicated logic circuits, but this naturally entails a corresponding increase in complexity of computation and analysis. Second, it is one of the early successes of synthetic biology [9]. Third, its resolution requires a global understanding of the dynamics of the design, and hence is a nontrivial mathematical problem. While experimental implementation of a design consisting of two mutually repressing transcription factors was a great triumph of predictive modeling, the design of [9] seems to be fragile and follow-up attempts [19] have been made to make it more robust. A natural question arises if more complex networks are able to exhibit a more robust switching behavior. This paper provides an efficient algorithmic approach towards addressing this question.

We begin with the well established observation that in vivo gene regulatory networks operate under noisy conditions [7, 21]. Rather than attempting to provide a specific model for the noise, we adopt the perspective that noise is significant enough to impact the initial conditions of the dynamics and the parameter values at which the network operates, but not so significant that it overwhelms the underlying nonlinear dynamics. Thus, for this paper we adopt the following *design principle*: a synthetic network should attempt to maximize the range of the phase space and parameter space where it exhibits the desired function.

Figure 1(b) summarizes the minimal structure and functionality of an (ascending) hysteretic switch. As values of an input signal are increased from a low level, the output signal is *off*. Once the input signal achieves a given threshold, S_1 , the output signal changes to *on* and remains at *on* for high values of the signal. As the input signal is lowered the output value remains *on* until the input signal reaches the threshold S_0 , that is lower than S_1 , at which point the output signal switches to *off*.

This property of “remembering” past states is called *hysteresis*. Since *on* and *off* are determined by dynamics, they must be represented by stable states. To obtain hysteresis requires that both stable states be present for the range of signal between S_0 and S_1 , e.g. that the system exhibits bistability. For this reason a system of this type is often referred to as a *bistable switch*.

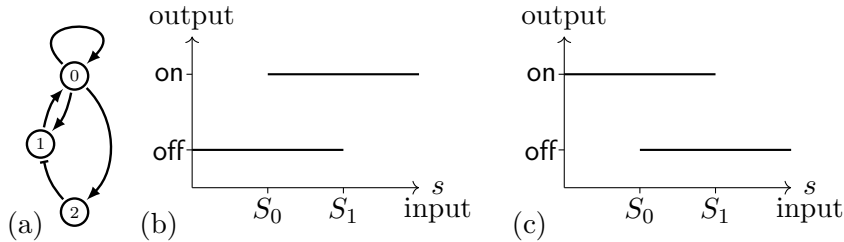


Figure 1: (a) Regulatory network 107. There are three nodes labelled 0, 1, and 2. Edges \rightarrow indicates up regulation and \vdash indicates down regulation. (b) Conceptual image of ascending hysteresis. Off/low output for low values of input signal s . On/high output for high values of s . Bistability for intermediate values of s allowing for hysteresis. (c) Descending hysteresis. Results, analogous to those for ascending hysteresis, are discussed in the supplementary material.

In order to have a well defined problem we ask and provide answers to the following question: Which three-node networks exhibit the functionality of a bistable switch over the largest range of parameter values? The reader is no doubt aware that as of yet we have not described our model for the network dynamics and not indicated what signals indicate on and off. This is discussed

in greater detail in later sections. For the moment we remark that the DSGRN model is based on combinatorics that can be justified mathematically using order theory and algebraic topology. The combinatorics allows us to perform extremely efficient computations, and as indicated above, allows DSGRN to be agnostic to the biochemical or biophysical details. Of course, it is precisely these details that play essential roles in the actual construction of components of a synthetic network. With this in mind, the true novelty of DSGRN is that it employs ideas from computational algebraic geometry to provide an explicit decomposition of parameter space [6, 17] on which dynamics is understood. It is unreasonable to expect that these precise bounds on parameters should be valid for more traditional models involving explicit nonlinearities. Nevertheless, as we demonstrate in the context of ordinary differential equation (ODE) models using Hill function nonlinearities with more than 20 dimensional parameter spaces, DSGRN provides considerable insight into parameter values at which bistable switching occurs.

2 Results

Our goal is to identify three-node networks that act as bistable switches over large regions of parameter space. As indicated in Figure 1(a) we label the nodes in our network by 0, 1, and 2, and assume that node 0 is directly effected by the input and the output of the network is expressed via node 2. Since each node can influence any other node (itself included) in three ways – activation, repression, or no impact – there are $3^9 = 19,683$ distinct three node networks. We exclude 5,103 trivial networks as defined in Methods 4.5. The number of regions into which DSGRN decomposes parameter space grows rapidly with the number of edges in the network. For example, three-node networks with 8 edges can have up to 823,011,840 distinct parameter regions, while for 9 edges this number increases to 93,329,542,656. Because of this size, we only consider one network with 9 edges, that where each edge is an activator. Therefore, we consider 14,068 networks. These networks are analyzed using the DSGRN software described in Section 4. For the purpose of reporting the results the following information suffices.

- I1** For three node networks the phase space is $\{(x_0, x_1, x_2) \mid x_n > 0\}$ where the variable x_n is associated with node n . For a given parameter value DSGRN decomposes phase space into cubes defined by the hyperplanes $x_n = \theta_{m,n}$ where $\theta_{m,n}$ is the threshold parameter associated with an edge from node n to node m . The global dynamics at the given parameter value is determined by a *state transition graph* defined on these cubes. A cube C that has a self edge

under the state transition graph is labeled as an $\text{FP}(i_0, i_1, i_2)$. This should be interpreted as a stable state under the associated dynamics. The $i_k \in \{0, 1, 2, 3\}$ indicates that if $x \in C$, then x_k is greater than i_k of the thresholds $\theta_{*,k}$, and thus provides information about the location in phase space of the stable state.

- I2** The parameter space for the DSGRN model consists of multiple positive real numbers associated with each node (1 for the node, 2 for each incoming edge, and 1 for each outgoing edge). For node n the DSGRN software produces a finite decomposition of parameter space and encodes this decomposition via a *factor graph*, denoted by $PG(n)$. Two vertices in the factor graph are connected by an edge if they represent regions of the continuous parameter space whose closures intersect on a codimension-one face.

Details about the parameters are presented in Methods 4.1. For the moment we remark that if at a vertex in the factor graph parameters associated with the in-edges do not align properly (i.e. the parameters corresponding to the in-edges are consistently too high, or consistently too low) with the parameters associated with the out-edges, then one can remove edges associated with the node. This in turn implies that the dynamics is captured by a simpler regulatory network. A node in the factor graph is defined to be *essential* if every in-edge and every out-edge are relevant for the dynamics [11]. The essential factor graph $PG_e(n)$ is the subgraph of the factor graph $PG(n)$ consisting of the essential nodes.

- I3** The full parameter space of a regulatory network is a product of the parameter spaces associated with each node. The decomposition of the full parameter space is indexed by the *parameter graph* PG . Since each region of this decomposition is made up of the product of the region from the decomposition of the parameter space of each node, the parameter graph is the product of the factor graphs, i.e. $PG = \prod_{n=0}^2 PG(n)$. Of fundamental importance is the fact that for each node in the parameter graph the state transition graph is constant over all parameters in the associated region. For each node in the parameter graph the DSGRN output includes the $\text{FP}(i_0, i_1, i_2)$ that arise from the associated state transition graph.

Fix a regulatory network with a fixed set of parameter values. In particular, this identifies a unique vertex (v_1, v_2) in the graph $PG(1) \times PG(2)$. Since we are interested in a direct correspondence between network topology and bistable switching we restrict our attention to the essential nodes $PG_e(1) \times PG_e(2)$. We view the continuous change of the input signal s to node 0 as a curve through the parameter space associated with node 0, e.g. monotone change in inducer concentration induces a monotone change in abundance of protein produced by gene 0 (cf. IPTG in [9]).

The DSGRN analogue to a continuous change in the inducer is a discrete path $v_0^0, \dots, v_0^t, \dots, v_0^T$ within the factor graph $PG(0)$, which is realized in the entire parameter graph as a path $(v_0^0, v_1, v_2), \dots, (v_0^t, v_1, v_2), \dots, (v_0^T, v_1, v_2)$ within the graph $PG(0) \times (v_1, v_2)$. Each vertex (v_0^t, v_1, v_2) on this path is an element of the parameter graph PG and hence for each vertex DSGRN can determine the global dynamics.

We say the path *exhibits ascending hysteresis* if at the initial vertex of the path (v_0^0, v_1, v_2) there is a $\text{FP}(i_0, i_1, j_1)$, at the final vertex of the path (v_0^T, v_1, v_2) there is a $\text{FP}(i_0, i_1, j_3)$ where $j_3 > j_1$, and at some intermediate vertex of the path there are two stable states $\text{FP}(i_0, i_1, j_1)$ and $\text{FP}(i_0, i_1, j_2)$ with $j_2 > j_1$. For the purposes of this paper we set $j_1 = 0$ and require that $j_2 > 0$ and $j_3 > 0$. Note that since we need to observe at least three distinct forms of global dynamics we insist that our paths be of length at least three.

Since such a path need not traverse all of $PG(0)$ we refer to it as a *partial path*. We focus on partial paths because we do not presume to know the parameter values associated to node 0 at which the regulatory network is acting in the absence of the input signal (cf. in the context of

construction of the toggle switch [9] we do not presume to know the level of protein production in the absence of the added IPTG).

We define the *hysteresis score* of a regulatory network to be the percentage of paths that exhibit ascending hysteresis among all paths. The total number of the paths is given by the number of paths of length at least 3 in $PG(0)$ times the total number of vertices in $PG_e(1) \times PG_e(2)$.

The ranking according to the hysteresis score is presented in Figure 2 (left). Observe that the typical three-node network is incapable of exhibiting hysteresis and less than 1% of networks are capable of producing hysteresis for the majority of parameter values. However, fourteen networks are capable of producing hysteresis for more than 60% of the paths. Based on our design principle we now restrict (for the most part) our attention to these fourteen three-node regulatory networks shown in Figure 3.

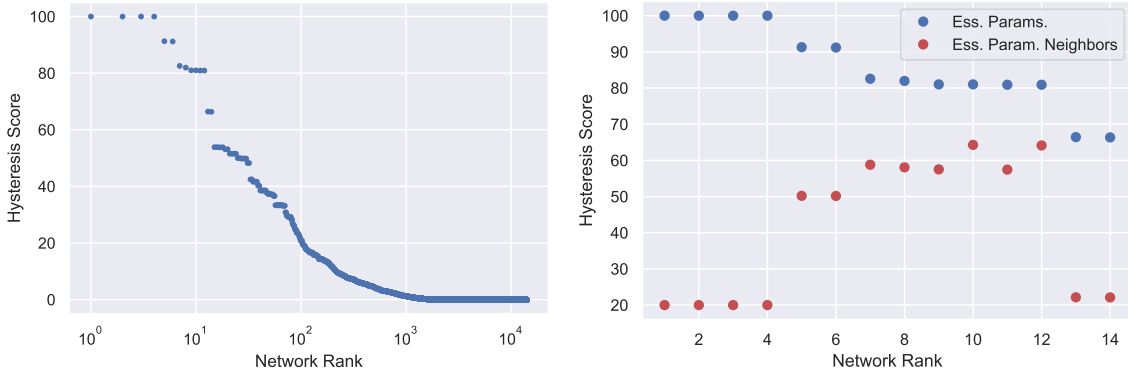


Figure 2: Left: 14,098 three node networks ranked by (ascending) hysteresis score analyzed at the essential parameters. This is the percentage of partial paths in the essential parameter sub-graph which exhibit switch-like behavior. The rapid decrease in score indicates that most networks are unlikely to exhibit hysteresis at most parameters. Right: The top scoring networks are further discriminated by scoring hysteresis in a neighborhood of the essential parameters. The scores after perturbation (red) are significantly lower than the scores at essential parameters (blue) for the top 4 networks. This is an indication that these networks are fragile i.e. will fail to perform well if any component of the network is removed. Networks with smaller gaps between red and blue scores indicate robust networks.

Returning to the motivation of our design principle that in vivo gene regulatory networks operate under noisy conditions, we remark that by restricting our analysis to essential nodes we are assuming that even under noisy conditions each edge of the regulatory network operates effectively. For example, networks 1-4 in Figure 3 have a partial path hysteresis score of 100% since they exhibit partial path hysteresis in all of their essential parameter nodes. However, it is clear that if any one of the edges is removed, the remaining network will not be bistable and not capable of hysteresis. This observation motivates search for a measure of the robustness of hysteresis with respect to network perturbations.

A more reasonable assumption might be that not all edges in the regulatory network function effectively at all times. To capture this, for the top fourteen regulatory networks we consider the set of parameter nodes in $PG(1) \times PG(2)$ that are within one edge of $PG_e(1) \times PG_e(2)$ and repeat the computation of the partial path hysteresis score. The results – we call this the *perturbed hysteresis score* – are shown in red in Figure 2 (right).

As expected, the perturbed hysteresis score is less than the hysteresis score. However, this loss of functionality varies widely across networks and is difficult to predict from the topology alone.

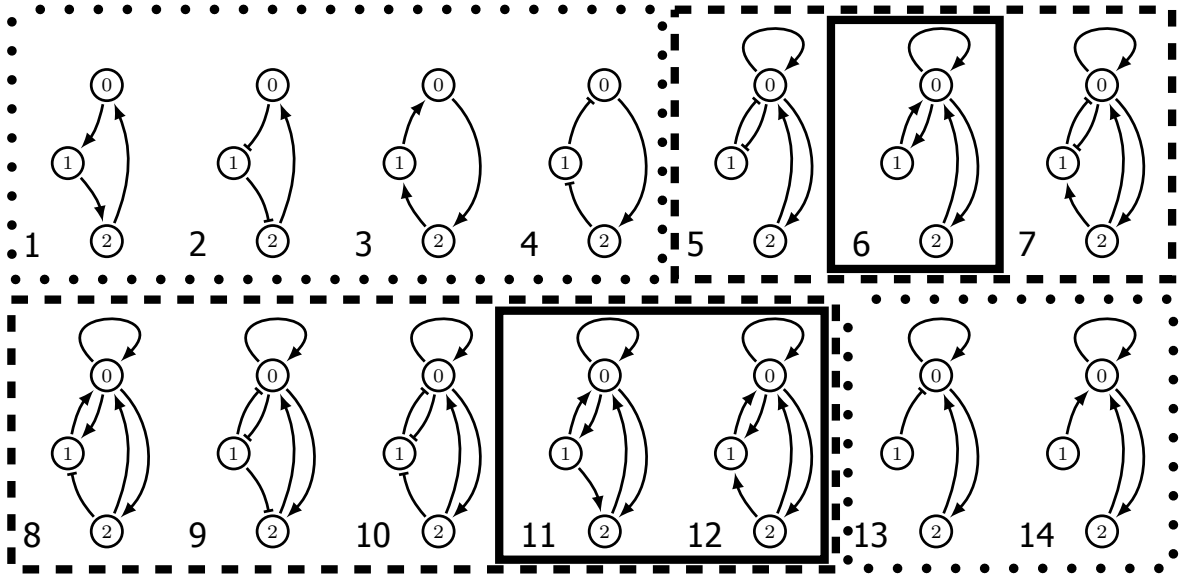


Figure 3: The top fourteen regulatory networks by hysteresis score. The six regulatory networks in dotted boxes are fragile, while the eight outlined via the dashed lines are robust. Observe that the three networks outlined by the solid lines are also consistent and each node acts only as an activator.

We define the *robustness score* of a regulatory network to be its perturbed hysteresis score divided by its hysteresis score. We refer to each network by its position in the list ordered by decreasing hysteresis score (see [8]). Networks 1-4, 13, and 14 (boxed with dotted lines in Figure 3) have robustness scores under 0.5. This suggests that under ideal conditions these networks will perform well as a switch. However, they are easy to break in the sense that small perturbations from the essential parameters largely destroy their ability to act as a switch. With this in mind we call regulatory networks with robustness score less than or equal to 0.5 *fragile*, while those scoring above 0.5 are referred to as *robust* (and are boxed by dashed lines in Figure 3).

Invoking the hysteresis rank and robustness allows us to reduce our attention to eight regulatory networks at which point we can focus on the actual topology of the design. The implementation of a gene regulatory network is constrained by available control mechanisms which must be considered when comparing networks. For instance, Network 5 in Figure 3 requires that node 0 act both as an activator and repressor. While this is biologically possible, e.g. the dimer CI acting in phage λ lysogenic/lytic switch, simpler design features may be desired. We call a node *consistent* if it acts as an activator or a repressor, but not both. As is indicated by the solid boxes in Figure 3 there are three high ranked and robust regulatory networks in which all nodes are consistent: 6, 11, and 12.

Note that in the networks 13 and 14, node 1 provides a constant input to node 0. Therefore node 1 does not affect the existence of ascending hysteresis. Removing this ineffectual node transforms networks 13 and 14 into a two node toggle switch with mutually activating edges, and with positive self-regulation on node 0. The fact that these networks are fragile in our analysis recapitulates the observation from [9, 19] that the two-node design of the toggle switch is fragile.

It is interesting to observe that the top three consistent regulatory networks that provide ascending hysteresis are based on nodes that are activators. The consistent regulatory network based on repressing nodes that has the highest hysteresis score (33.33%) is shown in Figure 4. This is a

fragile network with the perturbed hysteresis score of 6.66%

Thus, simple robust design of ascending hysteresis seems to require the use of activators. Interestingly, the role of activators in ascending hysteresis is not mirrored by the role of repressors in the descending hysteresis. First, no 3-node network that only consists of activators is capable of producing descending hysteresis. Second, in contrast with Figure 3, there is no network among the top 14 networks for descending hysteresis, with only repressing edges (see Figure S2 in the supplementary material).

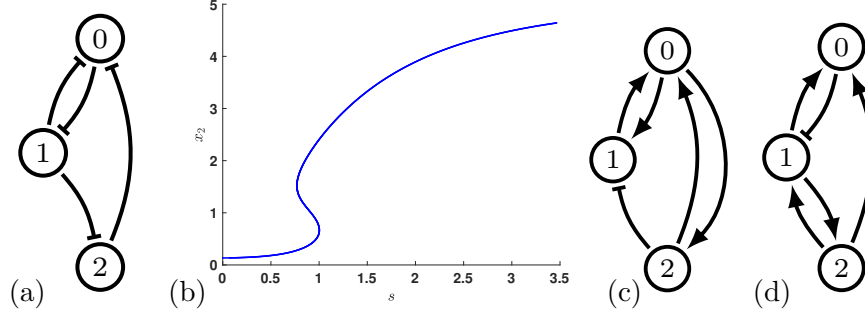


Figure 4: (a) The best network with only repressing edges, network 66, has a hysteresis score of 33.33%. (b) Continuation of equilibria in the Hill model (1) for regulatory network 12 using $n = 4$. (c) Regulatory network 33. (d) Regulatory network 3839.

Based on three criteria – hysteresis score, robustness score, and consistency of nodes – Network 12 is the most desirable design. Returning to the question posed in the introduction – are more complex networks capable of exhibiting more robust switching behavior – the answer is a qualified yes. However, complexity alone is not sufficient. This is evidenced by the fact that if Network 12 is modified by adding an additional activating edge from node 1 to

node 2, a self activation for either 1 or 2, or any combination of these edges the resulting network has a smaller hysteresis score, often dramatically so. For instance if we attempt to maximize complexity by adding every single edge as an activator, the resulting network has a hysteresis score of 0%.

The results discussed up to this point have all been obtained from the combinatorial computations of DSGRN. More traditional modeling of regulatory networks is based on ODEs. As is discussed in Methods 4.1 and Supplementary Material B there is a direct translation from DSGRN parameters to nonlinearities based on Hill functions in the limit when the exponents in the Hill function are very large. We now demonstrate that information from DSGRN has implications for the ODE models. Two important observations are that (i) trustworthy ODE computations are many orders of magnitude more expensive than DSGRN computations, and (ii) it is unreasonable to expect the explicit DSGRN decomposition of parameter space to apply precisely to any specific ODE.

To expand on this we consider Network 12 and the corresponding ODE

$$\begin{aligned} \dot{x}_0 &= -\gamma_0 x_0 + L_0 + \frac{\delta_{0,0} x_0^n}{\theta_{0,0}^n + x_0^n} + \frac{\delta_{0,1} x_1^n}{\theta_{0,1}^n + x_1^n} + \frac{\delta_{0,2} x_2^n}{\theta_{0,2}^n + x_2^n} + s \\ \dot{x}_1 &= -\gamma_1 x_1 + L_1 + \frac{\delta_{1,0} x_0^n}{\theta_{1,0}^n + x_0^n} + \frac{\delta_{1,2} x_2^n}{\theta_{1,2}^n + x_2^n} \\ \dot{x}_2 &= -\gamma_2 x_2 + L_2 + \frac{\delta_{2,0} x_0^n}{\theta_{2,0}^n + x_0^n} \end{aligned} \quad (1)$$

where for simplicity have made two modeling assumptions. First, the effect of the external signal on the growth rate of x_0 is given by a simple linear additive term s . Second, the exponents n of

the Hill functions are the same. In addition, there are 21 other parameters that lie in $(0, \infty)^{21}$ (see Methods 4.1). There are 707 vertices in $PG(0)$ (see [6, Table 1]), and 24 vertices in $PG_e(1) \times PG_e(2)$ (see Methods 4.4).

The most computationally efficient means of identifying the desired hysteresis curve in (1) is to fix a parameter value in $(0, \infty)^{22}$, choose an initial value s_0 for s , find a stable fixed point with low x_2 value, perform continuation with respect to arc-length of a fixed length, and check that two saddle-node bifurcations have occurred. An example of this computation is shown in Figure 4(b) (see Supplementary Materials for details). With the goal of quantifying how robustly this system exhibits hysteresis the obvious question is how many parameter values should be chosen and what is the appropriate choice of arc-length. Based on the number of vertices in $PG(0)$ and $PG_e(1) \times PG_e(2)$, the number of partial paths computed by DSGRN is on the order of 10^5 . Furthermore, since each region of parameter space is an unbounded open set in $(0, \infty)^{22}$ even sampling each region is non-trivial. This suggests that performing sufficiently many continuation computations to compare with the DSGRN hysteresis score is prohibitively expensive.

With this in mind we greatly simplify the DSGRN computations being performed. We remark that a partial order can be placed on the vertices of $PG(0)$ (see Methods 4.1) such that there is a unique minimal vertex \underline{v}_0 and unique maximal vertex \bar{v}_0 . A path $v_0^0, \dots, v_0^t, \dots, v_0^T$ within the factor graph $PG(0)$ is *full* if $v_0^0 = \underline{v}_0$ and $v_0^T = \bar{v}_0$. This leads to two new scores obtained as follows.

For each vertex in $(v_1, v_2) \in PG_e(1) \times PG_e(2)$ we consider all full paths

$$(\underline{v}_0, v_1, v_2), \dots, (v_0^t, v_1, v_2), \dots, (\bar{v}_0, v_1, v_2)$$

and mark those paths that exhibits hysteresis as hysteretic. The *full path hysteresis score* is the percentage of hysteretic paths among all full paths. The *perturbed full path hysteresis score* is the same but based on the one edge neighborhood of $PG_e(1) \times PG_e(2)$.

To compare the predictions of DSGRN against ODE models we chose four regulatory networks, Network 12 from Figure 3, Network 107 from Figure 1(a), and Network 33 and 3839 shown in Figure 4(c) and (d). These latter three networks were chosen because they exhibit different hysteresis scores: 42.46%, 18.95%, and 0%, respectively. For each network we performed two sets of experiments. For the first we randomly chose 1000 parameter values that lay in $\underline{v}_0 \times PG_e(1) \times PG_e(2)$, and for the second we chose 1000 parameter values in the one edge neighborhood with respect to $PG_e(1) \times PG_e(2)$. In each case for each parameter choice we performed the above mentioned procedure to identify whether or not one obtains a hysteresis curve. The results are indicated in Table 1.

We highlight three observations from Table 1.

- *For large Hill exponent n the DSGRN full path scores and the ODE scores are quite similar.* This is not surprising. DSGRN is based on a mathematical approach to nonlinear dynamics that captures robust features [13, 15, 14, 16, 12].
- *For more biologically realistic levels of n the quantitative agreement between the scores disappears.* Again, this is not surprising. It has long been known that in order for nonlinearities with gentle sigmoidal shape to intersect at multiple points, their parameters must be carefully adjusted. As a result, for low n , bistability is rare.
- *The relative ranking by DSGRN of the capability of regulatory networks to achieve robust switching is predictive of the observations from the ODE models.* Moving from left to right along the rows, DSGRN predicts that the corresponding networks are progressively less capable of acting as a robust switch. For the most part the ODE simulations agree with this

Regulatory Network	12		33		107		3839	
Hill function exponent n	Unperturbed Score	Perturbed Score	Unperturbed Score	Perturbed Score	Unperturbed Score	Perturbed Score	Unperturbed Score	Perturbed Score
30	96.4 %	72.2 %	84.8 %	34.5 %	29.7 %	57.1 %	6.8 %	3.8 %
20	92.2 %	58.1 %	78.5 %	30.2 %	16.7 %	42.9 %	7.3 %	4.5 %
10	68 %	26.3 %	50 %	16.9 %	2.8 %	16.1 %	7.8 %	3.6 %
5	17.7 %	3.6 %	12.4 %	3.4 %	0 %	2.3 %	7.5 %	2.1 %
4	8.9 %	1.6 %	6.1 %	1.4 %	0%	0.5 %	4.4 %	1.2 %
DSGRN (full path)	100 %	79.09 %	83.33 %	61.67 %	33.96 %	25.05 %	0 %	0 %
DSGRN (partial path)	80.91 %	64.13 %	42.46 %	27.73 %	18.95 %	13.34 %	0 %	0 %

Table 1: The Regulatory Network number comes from the ranking of the hysteresis score [8]. The bottom two rows indicate the full path and partial path hysteresis scores obtained from DSGRN. The first column indicates the exponent of the Hill function used in the ODE model for the regulatory network, e.g. (1). The two columns under each regulatory network number indicate the percentage of continuation computations that result in a hysteresis curve. The first column assumes the parameter value is in a region defined by $\underline{v}_0 \times FP(1) \times FP(2)$ and the second column assume the parameter value is in region defined by a one edge neighborhood. 1000 curves were computed for each entry.

prediction. Most importantly, Network 12 is the best at all values of n . We include Networks 107 and 3839 to emphasize that the predictive power of DSGRN is not perfect. However, for these networks the realization of ascending hysteresis is consistently low, again suggesting that DSGRN is capable of identifying regulatory networks of interest.

3 Discussion

DSGRN provides a modeling framework and associated computational tool that is capable of analyzing all 3-node regulatory networks for prevalence over a large range of parameter values of a particular phenotype. Our investigation into the identification of the robust expression of the phenotype of hysteresis demonstrates DSGRN’s practical value – in synthetic biology hysteresis forms a basis for a design of a bistable switch. It also demonstrates the power of DSGRN to capture complex dynamics – hysteresis arises from global organization of multiple phenotypes (monostability, bistability, monostability) as a function of increasing external input. Furthermore, the publicly available searchable database of all 3-node networks allows synthetic biologist to select robust designs that meets additional implementation criteria [8].

It is important to note that the complexity of hysteresis phenotype makes it challenging to succinctly describe the network features i.e. number, sign and position of edges, that characterize high scoring networks. While it is known that presence of positive edges generally leads to bistability, our computations show that there is no simple relationship between the hysteresis score and the number of positive edges. Furthermore, we believe that as size and complexity of networks increase, simple network features are even less likely to predict presence or absence of specific dynamics. Thus, a direct evaluation of the prevalence of such dynamics across parameters by DSGRN becomes a crucial tool in understanding of behavior of complex networks.

Obviously, DSGRN can be used to search for simpler phenotypes. In particular, it has been used to catalog types and number of intermediate steady states in epithelial-mesenchymal transition network [22], as well as to characterize START network controlling G1/S transition in human cell

cycle [11]. In principle it can be applied to the analysis of more complicated control circuits.

DSGRN occupies a novel niche in the collection of modeling tools for regulatory networks. Similar to Boolean models it is based on a combinatorial expression of dynamics and thus lends itself to extremely efficient computations. The goal of DSGRN is not to precisely match and reproduce carefully measured expression data of genes over a wide variety of growth conditions. However, in the setting of systems biology more often than not such measurements are not available, in particular for networks involving more than a few genes. In such situations, DSGRN can be a first step in understanding of network dynamics. DSGRN can search through many proposed networks over a wide range of parameter values, and eliminate those that do not support the desired dynamical behavior, coarsely defined e.g. equilibria or oscillations with particular patterns of high and low expression values. Elimination of networks or reduction of potential functional parameter values for a given network provides significant reduction of hypotheses space.

In contexts where one has carefully measured expression data of genes, modeling tools of choice often involve ODEs with experimentally determined parameters. In contrast to Boolean approach, the mathematical foundations of DSGRN – a continuous phase space and parameter space – allows for direct comparison with ODE models. As is demonstrated in this paper, DSGRN provides a means to compare systems of ODEs. In particular, it can rank the relative ability of ODE models to produce particular dynamics over large ranges of parameter values. At the same time, DSGRN provides a priori bounds on parameter regions where sampling of parameters and fitting the expression data is feasible. Finally, DSGRN provides, at low computational cost, the ability to describe relationships between any simultaneous change in many parameters and the changes in network dynamics. This facilitates generation of hypothesis of behavior of a system under different conditions and leads to prioritization of experiments.

To add additional emphasis on the importance of the computational efficacy of DSGRN we note that the comparisons in Table 1 are based on full path and perturbed full path hysteresis scores. We expect that in many applications it is more likely that external control will not lead to a path that extends across the entire parameter domain of the input node. In this case the partial path statistics are more relevant. However, carrying out such computations in the setting of traditional ODE models appears to be computationally prohibitive.

Due to its ability to describe complex relationship between network parameters and network dynamics, albeit on a coarse level, and the associated systematic reduction of the hypothesis space for experimental examination of this dynamics, DSGRN should become a part of an essential toolbox in systems and synthetic biology.

4 Methods

We provide a brief description of how DSGRN combinatorializes both phase space and parameter space of regulatory networks. For more details the reader is referred to [6, 11, 10].

4.1 Input and Output

DSGRN takes as input an annotated directed graph (see Figure 3), called a *regulatory network*, where the annotations on the edges indicate activation \rightarrow or repression \neg along with an algebraic expression that indicates how incoming edges to a node interact. For this paper we first add rates associated with \rightarrow edges and then multiply by values associated with \neg edges. With this input DSGRN is capable of producing as output a queryable database, called the *DSGRN database*, indicating the possible global dynamics at associated parameters. Conceptually it is useful to view the DSGRN database as a graph, called the *parameter graph*, where associated to each node in the

parameter graph is an explicit region in parameter space and a description of the global dynamics in the form of a *Morse graph* (described below). For a fixed ordering of the thresholds (see below), an edge between two nodes in the parameter graph indicates that the associated regions share a co-dimension 1 boundary.

Implicit in the DSGRN calculations is that there is a positive variable x_n , e.g. level of protein, associated with node n of the regulatory network. The dynamics of x_n is controlled by the following parameters. Each x_n decays at a rate γ_n . If there is an edge from node m to node n , then the model includes three positive parameters: $\ell_{n,m}$, a low growth rate of x_n induced by x_m ; $\delta_{n,m}$, such that $\ell_{n,m} + \delta_{n,m}$ represents a high growth rate of x_n induced by x_m ; and $\theta_{n,m}$, a *threshold* that separates the values of x_m that induce low or high growth rate of x_n . Thus the parameter space for a regulatory network with N nodes and E edges is $(0, \infty)^{N+3E}$.

4.2 Combinatorial Dynamics

Note that if there are s_n out-edges from node n , there must be s_n thresholds associated to node n with indices of the form, $\theta_{*,n}$, and these thresholds divide the domain of the variable, x_n , into $s_n + 1$ intervals. This in turn implies that for a given regulatory network with N nodes there is a decomposition of the phase space $(0, \infty)^N$ into rectangular cells bounded by thresholds, zero, or extending to infinity.

Each cell is labeled by a vector $(\alpha_0, \alpha_1, \dots, \alpha_{N-1})$, $\alpha_n \in \{0, \dots, s_n\}$, where $s_n \in \{0, \dots, N\}$ is the number of out-edges of node n in the network under consideration. See Figure 5(a) for an illustration for a three node network i.e. $N = 3$.

The combinatorial dynamics is represented by a *state transition graph* (STG) as defined in [6]. Each node of the STG represents one rectangular cell and edges indicate how cells are mapped forward in time.

As presented in [6], DSGRN was not capable of analyzing networks with self repressing interactions or nodes without an out-edge. As part of the present work we remove these restrictions (see Supplementary Material for details). The code is available at [5].

4.3 Morse graphs

The information in the STG is summarized by a *Morse graph*. This is an acyclic directed graph, or, equivalently, a partially ordered set, where nodes indicate potential recurrent dynamics and the directed edges indicate the direction of the dynamics between recurrent sets [2, 6]. We summarize the importance of Morse graph representation of dynamics by noting that any *minimal* node of the Morse graph labeled $FP(\alpha_0, \alpha_1, \alpha_2)$ indicates that the corresponding cell is an attracting region for the dynamics [6]. Thus a Morse graph with a unique minimal node suggests monostability, while two minimal nodes indicates bistability.

4.4 Parameter graph

The DSGRN parameter space, $(0, \infty)^{N+3E}$, is represented by the parameter graph PG . Each node of the parameter graph corresponds to an explicit open semi-algebraic set [6] with the property that the STG is constant for all parameters in that set. In particular, there is a unique Morse graph associated to each node in the parameter graph.

As is discussed in **I2** and **I3** the parameter graph is the product of the factor graphs and each factor graph is determined by the in-edges and out-edges of its corresponding node in the regulatory network. Figure 5(b) shows the factor graphs for nodes whose number of in and out-edges are (from left to right) $(2, 1)$, $(1, 2)$, and $(1, 1)$.

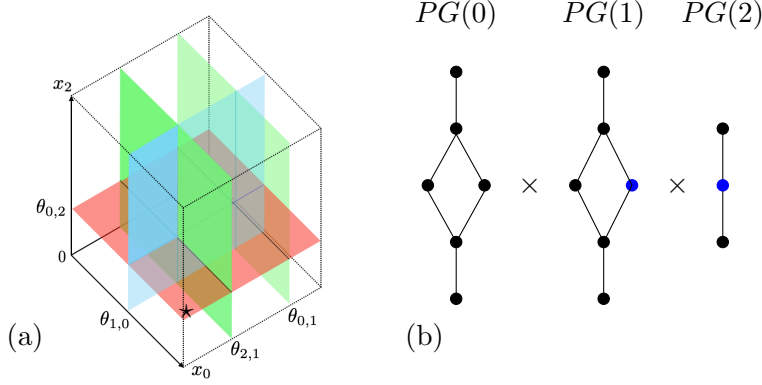


Figure 5: (a) Phase space decomposition for Regulatory Network shown in Figure 4(a) under the assumption that $\theta_{2,1} < \theta_{0,1}$. The cell identified by \star is labeled $(1,0,0)$. (b) For fixed ordering of the thresholds the parameter graph for the network in Figure 4(a) where the nodes 0, 1, and 2 have 2 in-edges and 1 out-edge, 1 in-edge and 2 out-edges, and 1 in-edge and 1 out-edge, respectively, written as a Cartesian product of the three factor graphs. For $i = 1, 2$, $PG_e(i)$ is the subgraph consisting of only the blue vertices.

General descriptions of how parameters are identified with nodes of the factor graph can be found in [6, 17]. To provide intuition we focus on the simplest factor graph corresponding to $(1,1)$. Because there is a single in-edge and a single out-edge, there is a unique γ , θ , ℓ and δ (see Section 4.1). The nodes in the factor graph (from bottom to top) are associated with the inequalities

$$\gamma\theta < \ell < \ell + \delta, \quad \ell < \gamma\theta < \ell + \delta, \quad \ell < \ell + \delta < \gamma\theta.$$

Observe that the order of this set of inequalities can be obtained by associating it with increasing the values of γ . This same approach applies in general and thus induces a partial order on any form of factor graph that $PG(0)$ may assume. All full and partial paths discussed in Section 2 are chosen to be strictly monotone with respect this partial order.

4.5 Constraints on searched networks

There are $3^9 = 19,683$ three node networks. We only consider a subset of these defined as follows. Let $a_{ij} \in \{-1, 0, 1\}$ denote the *edge coefficients* which describe the type (or lack) of interaction from node j to node i . Specifically, $a_{ij} = 0$ if there is no interaction, $a_{ij} = -1$ if node j represses node i , and $a_{ij} = 1$ if node j activates node i . We say that a three node network is *trivial* if either there exists no path from node 0 to node 2, or no path from node 1 to node 2. In terms of the edge coefficients, a network is trivial if and only if

$$|a_{20}a_{21}| + |a_{20}a_{01}| + |a_{21}a_{10}| = 0.$$

Our restriction to nontrivial networks follows from the observation that if a network has no path from node 0 to node 2, then it is incapable of acting as a switch. Furthermore, if there is no path from node 1 to node 2, then node 1 has no influence on the dynamics, and therefore can not be responsible for any hysteresis or lack thereof. We omit these 5,103 trivial networks from our analysis.

As indicated in the introduction we omit all but one of the three node networks in which every gene interacts directly with every other gene. The remaining 14,068 are the networks analyzed in this paper.

4.6 Computations

The computations of the DSGRN ascending hysteresis score presented in Figure 2 took a total wall time of 1,478.61 hours. The computations were performed on a cluster with 100 nodes and finished after just over 15 hours. The numerical continuation for Hill models presented in Table 1 were computed on a single laptop and took a total time of 7.9 hours.

Acknowledgements

The work of M.G., S. K., and K.M. was partially supported by the National Science Foundation under awards DMS-1839294 and HDR TRIPODS award CCF-1934924, DARPA contract HR0011-16-2-0033, and National Institutes of Health award R01 GM126555. The work of M.G. was partially supported by FAPESP grant 2019/06249-7 and by CNPq grant 309073/2019-7. The work of T. G. was partially supported by NSF grant DMS-1839299, DARPA FA8750-17-C-0054 and NIH 5R01GM126555-01. The authors thank Bree Cummins for helpful discussions.

References

- [1] LB. Andrews, AAK. Nielsen, and CA. Voigt. Cellular checkpoint control using programmable sequential logic. *Science*, (361):eaap8987, 2018.
- [2] Zin Arai, William Kalies, Hiroshi Kokubu, Konstantin Mischaikow, Hiroe Oka, and Paweł Pilarczyk. A database schema for the analysis of global dynamics of multiparameter systems. *SIAM J. Appl. Dyn. Syst.*, 8(3):757–789, 2009.
- [3] JJ Bashor, CJ abd Collins. Understanding biological regulation through synthetic biology. *Annu Rev Biophys*, (47):399 – 423, 2018.
- [4] S. Basu, Y. Gerchman, CH. Collins, FH. Arnold, and R. Weiss. A synthetic multicellular system for programmed pattern formation. *Nature*, (434):1130–1134, 2005.
- [5] Shaun Harker Bree Cummins, Marcio Gameiro. DSGRN: Dynamic Signatures Generated by Regulatory Networks. <https://github.com/marciogameiro/DSGRN>, 2020.
- [6] Bree Cummins, Tomas Gedeon, Shaun Harker, Konstantin Mischaikow, and Kafung Mok. Combinatorial representation of parameter space for switching networks. *SIAM Journal on Applied Dynamical Systems*, 15(4):2176–2212, 2016.
- [7] Michael B. Elowitz, Arnold J. Levine, Eric D. Siggia, and Peter S. Swain. Stochastic gene expression in a single cell. *Science*, 297(5584):1183–1186, 2002.
- [8] Marcio Gameiro. Code supplemental for “rational design of complex phenotype via network models”. <https://github.com/marciogameiro/three-node-hysteresis>, 2020.
- [9] Timothy Gardner, Charles Cantor, and James Collins. Construction of a genetic toggle switch in *Escherichia coli*. *Nature*, 403(6767):339–342, 2000.
- [10] T. Gedeon. Multi-parameter exploration of dynamics of regulatory networks. *BioSystems*, 190:104113, 2020.

- [11] Tomas Gedeon, Bree Cummins, Shaun Harker, and Konstantin Mischaikow. Identifying robust hysteresis in networks. *PLOS Computational Biology*, 14(4):1–23, 04 2018.
- [12] Tomáš Gedeon, Shaun Harker, Hiroshi Kokubu, Konstantin Mischaikow, and Hiroe Oka. Global dynamics for steep nonlinearities in two dimensions. *Physica D: Nonlinear Phenomena*, 339:18–38, 2017.
- [13] W. D. Kalies, K. Mischaikow, and R. C. A. M. VanderVorst. An algorithmic approach to chain recurrence. *Found. Comput. Math.*, 5(4):409–449, 2005.
- [14] W. D. Kalies, K. Mischaikow, and R. C. A. M. Vandervorst. Lattice structures for attractors II. *Found. Comput. Math.*, 2015.
- [15] William Kalies, Konstantin Mischaikow, and Robert Vandervorst. Lattice structures for attractors I. *J. of Comp. Dyn.*, 1(2), 2014.
- [16] William D. Kalies, Konstantin Mischaikow, and Robert C. A. M. Vandervorst. Lattice structures for attractors iii, 2019.
- [17] Shane Kepley, Konstantin Mischaikow, and Lun Zhang. Computing linear extensions for boolean lattices with algebraic constraints. <https://arxiv.org/abs/2006.02622>, 2020.
- [18] T. Kitada, B. Diandreth, B. Teague, and R. Weiss. Programming gene and engineered-cell therapies with synthetic biology. *Science*, (359):eaad1067, 2018.
- [19] T. Lebar, U. Bezeljak, A. Golob, and et al. A bistable genetic switch based on designable dna-binding domains. *Nat Commun.*, (5):5007, 2014.
- [20] KD. Litcofsky, RB. Afeyan, RJ. Krom, AS. Khali, and JJ. Collins. Iterative plugand-play methodology for constructing and modifying synthetic gene. *Nat Method*, (9):1077–1080, 2012.
- [21] M Thattai and A van Oudenaarden. Intrinsic noise in gene regulatory networks. *Proceedings of the National Academy of Sciences of the United States of America*, 98(15):8614–9, 2001.
- [22] Y. Xin, B. Cummins, and T. Gedeon. Multi-stability in epithelial-mesenchymal transition network. *BMC Bioinformatics*, 21(71), 2020.

Supplementary Information for: Rational design of complex phenotype via network models

Marcio Gameiro* Tomáš Gedeon† Shane Kepley‡ Konstantin Mischaikow§

May 30, 2022

A Results for descending hysteresis

We consider *descending hysteresis* in which the switch-like behavior transitions from a high steady state to a low steady state with bistability in between. A schematic for this case is shown in Figure 1(c) of the main text.

We carried out the same analysis as for the ascending hysteresis. The combinatorial definition of descending hysteresis is analogous to that of ascending hysteresis. Specifically, a path exhibits descending hysteresis if at the initial vertex of the path (v_0^0, v_1, v_2) there is a $\text{FP}(i_0, i_1, j_1)$, at the final vertex of the path (v_0^T, v_1, v_2) there is a $\text{FP}(i_0, i_1, j_3)$ with $j_3 < j_1$, and at some intermediate vertex of the path there are two stable states $\text{FP}(i_0, i_1, j_1)$ and $\text{FP}(i_0, i_1, j_2)$ with $j_2 < j_1$. For the purposes of this paper we set $j_3 = 0$ and require that $j_1 > 0$ and $j_2 > 0$. As in the study of the ascending hysteresis, we only consider paths of length at least three.

The ranking according to the hysteresis score is presented in Figure S1 (left) along with the scores after perturbation for the top 14 networks in Figure S1 (right.) These 14 networks are shown in Figure S2. Observe the striking similarity with Figure 3 in the main text. In both cases there are exactly 4 networks that have a 100% hysteresis score and contain only 3 edges that cyclically connect the nodes. All of these networks are fragile and their corresponding robustness scores are also similar. Comparing Figure 2 of the main text with Figure S1 we observe that the distribution of ascending and descending hysteresis scores are very similar and indicate that robust switching is relatively rare in either case. The close similarity between analysis of the entire collection of 3 node networks with respect to ascending and descending hysteresis suggests that there exists some relation, e.g. symmetry, where a network's ascending hysteresis and robustness scores are comparable to its partner's descending scores. This relation does not appear to be obvious as it must be compatible with observations about asymmetry made in the main text. For example, even though there is a network consisting of only repressors that exhibits ascending hysteresis ranked networks, there is no network with only activators that exhibits descending hysteresis. Exploring this relationship and its implications is the subject of current research and remains an open problem.

*gameiro@math.rutgers.edu

†gedeon@math.montana.edu

‡sk2011@math.rutgers.edu

§mischaik@math.rutgers.edu

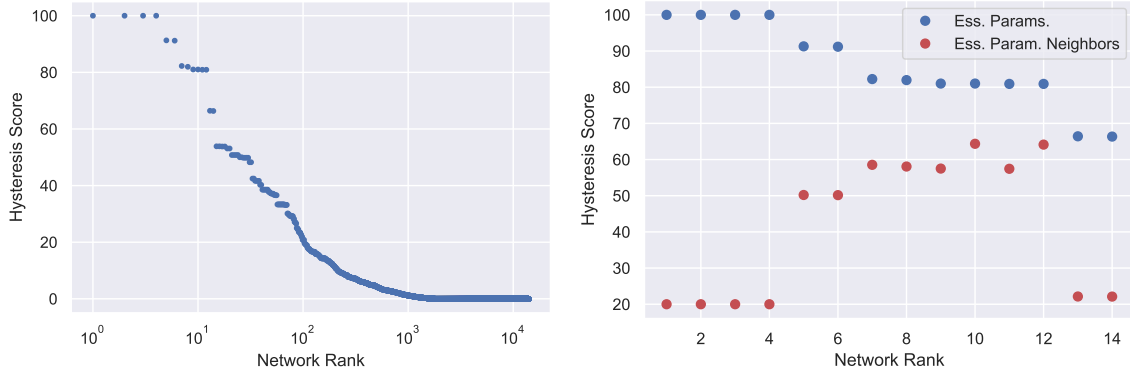


Figure S1: Left: 14,098 three node networks ranked by (descending) hysteresis score analyzed at the essential parameters. Right: The top scoring networks are further discriminated by scoring hysteresis in a neighborhood of the essential parameters. The scores after perturbation are shown in (red) and the scores at essential parameters in (blue).

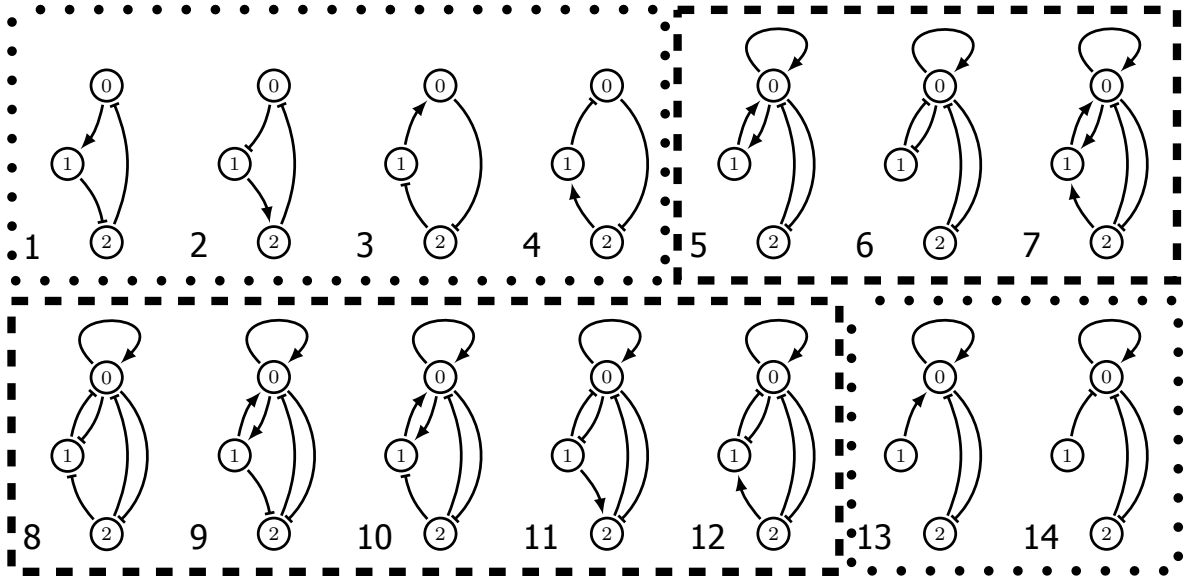


Figure S2: The top fourteen regulatory networks by descending hysteresis score. The six regulatory networks in dotted boxes are fragile, while the eight outlined via the dashed lines are robust. Observe that none of the networks are consistent. Networks 13 and 14 are analogous to networks 13 and 14 of the main paper. The fact that they are fragile recovers observation from [3] that 2-node toggle switch is fragile (see comment in the main text.)

B Hill model continuation computations

The dynamics of a regulatory network as modelled by DSGRN is obtained by assuming that the rate of change of x can be approximated by

$$-\Gamma x + \Lambda(x), \quad (1)$$

where $x = (x_0, \dots, x_{N-1})$ represent the state variables of the N nodes of the network, Γ is a diagonal matrix

$$\Gamma = \begin{pmatrix} \gamma_0 & & & \\ & \gamma_1 & & \\ & & \ddots & \\ & & & \gamma_{N-1} \end{pmatrix}$$

where $\gamma_i > 0$ is the decay rate of x_i , and $\Lambda(x) = (\Lambda_0(x), \dots, \Lambda_{N-1}(x))$ takes the form described below. Let

$$\sigma^+(y, \ell, \delta, \theta) = \begin{cases} \ell, & \text{if } y < \theta \\ \ell + \delta, & \text{if } y > \theta \end{cases}$$

and

$$\sigma^-(y, \ell, \delta, \theta) = \begin{cases} \ell + \delta, & \text{if } y < \theta \\ \ell, & \text{if } y > \theta. \end{cases}$$

Assume that node i has k in-edges from the nodes j_1, \dots, j_k in the regulatory network. Furthermore, assume that of these edges j_1, \dots, j_{k_1} are activating and j_{k_1+1}, \dots, j_k are repressing. For the computations of this paper we set

$$\Lambda_i(x) = \left(\sigma^+(x_{j_1}) + \dots + \sigma^+(x_{j_{k_1}}) \right) \sigma^-(x_{j_{k_1+1}}) \dots \sigma^-(x_{j_k}).$$

As an example, for network 12 in Figure 3 of the main text, (1) takes the form

$$\begin{aligned} & -\gamma_0 x_0 + \sigma^+(x_0, \ell_{0,0}, \delta_{0,0}, \theta_{0,0}) + \sigma^+(x_1, \ell_{0,1}, \delta_{0,1}, \theta_{0,1}) + \sigma^+(x_2, \ell_{0,2}, \delta_{0,2}, \theta_{0,2}) \\ & -\gamma_1 x_1 + \sigma^+(x_0, \ell_{1,0}, \delta_{1,0}, \theta_{1,0}) + \sigma^+(x_2, \ell_{1,2}, \delta_{1,2}, \theta_{1,2}) \\ & -\gamma_2 x_2 + \sigma^+(x_0, \ell_{2,0}, \delta_{2,0}, \theta_{2,0}) \end{aligned}$$

since all the in-edges are activating.

For the numerical computations to obtain the results in Table 1 in the main text and Table S1 we consider Hill function models

$$\begin{aligned} \dot{x}_0 &= -\gamma_0 x_0 + H_0(x) + s \\ \dot{x}_1 &= -\gamma_1 x_1 + H_1(x) \\ \dot{x}_2 &= -\gamma_2 x_2 + H_2(x) \end{aligned}$$

where H_i is obtained from the regulatory network by replacing the step functions σ^- and σ^+ in Λ_i by the decreasing and increasing Hill functions

$$H^-(x, \ell, \delta, \theta, n) = \ell + \delta \frac{\theta^n}{\theta^n + x^n}$$

and

$$H^+(x, \ell, \delta, \theta, n) = \ell + \delta \frac{x^n}{\theta^n + x^n},$$

Regulatory Network	12		33		108		4346	
Hill function exponent n	Unperturbed Score	Perturbed Score	Unperturbed Score	Perturbed Score	Unperturbed Score	Perturbed Score	Unperturbed Score	Perturbed Score
30	81.2 %	51.7 %	84.4 %	41.2 %	57.9 %	56.1 %	0 %	0 %
20	70.8 %	41.3 %	74.9 %	34.0 %	45.4 %	46.8 %	0 %	0 %
10	39.7 %	18.8 %	45.3 %	16.6 %	18.2 %	21.8 %	0 %	0 %
5	7.3 %	2.1 %	7.6 %	2.2 %	1.3 %	2.4 %	0 %	0 %
4	3.1 %	0.6 %	2.2 %	0.5 %	0.2 %	0.3 %	0 %	0 %
DSGRN (full path)	100 %	79.1 %	83.3 %	61.7 %	33.9 %	25.1 %	0 %	0 %
DSGRN (partial path)	80.9 %	64.1 %	42.5 %	27.7 %	18.9 %	13.3 %	0 %	0 %

Table S1: (Unperturbed and Perturbed Hysteresis Scores) Results for comparisons with four networks. Numbers for Regulatory network come from ranking in Figure S1. Bottom rows are the full and partial path hysteresis scores obtained from DSGRN for Regulatory networks 12, 33, 108, and 4346. The first column indicates the exponent of the Hill function used in the ODE model for the regulatory network. The two columns under each regulatory network number indicate the percentage of continuation computations that result in a hysteresis curve. The first column assumes the parameter value is in a region defined by $\underline{v}_0 \times FP(1) \times FP(2)$ and the second column assume the parameter value is in region defined by a one edge neighborhood. 1000 curves were computed for each entry.

respectively. We represent the input signal to node 0 by the additive parameter s in the first equation.

Returning to network 12 in Figure 3 of the main text, the Hill model is given by

$$\begin{aligned}
\dot{x}_0 &= -\gamma_0 x_0 + \ell_{0,0} + \frac{\delta_{0,0} x_0^n}{\theta_{0,0}^n + x_0^n} + \ell_{0,1} + \frac{\delta_{0,1} x_1^n}{\theta_{0,1}^n + x_1^n} + \ell_{0,2} + \frac{\delta_{0,2} x_2^n}{\theta_{0,2}^n + x_2^n} + s \\
\dot{x}_1 &= -\gamma_1 x_1 + \ell_{1,0} + \frac{\delta_{1,0} x_0^n}{\theta_{1,0}^n + x_0^n} + \ell_{1,2} + \frac{\delta_{1,2} x_2^n}{\theta_{1,2}^n + x_2^n} \\
\dot{x}_2 &= -\gamma_2 x_2 + \ell_{2,0} + \frac{\delta_{2,0} x_0^n}{\theta_{2,0}^n + x_0^n}.
\end{aligned}$$

Notice that in Eq. (1) of the main text we combined the ℓ parameters as $L_0 = \ell_{0,0} + \ell_{0,1} + \ell_{0,2}$, $L_1 = \ell_{1,0} + \ell_{1,2}$, and $L_2 = \ell_{2,0}$.

Using the Hill models we compute curves of equilibria using a pseudo arclength continuation method [4] to detect fold bifurcation points. A sample continuation curve for Eq. (1) of the main text is presented in Figure 4(b) in the main text, where the following values of parameters were used: $\gamma_0 = 1$, $\gamma_1 = 1$, $\gamma_2 = 1$, $L_0 = 0.508736659464953$, $L_1 = 0.823149364604282$, $L_2 = 0.129562882298977$, $\theta_{0,0} = 2.742699202456864$, $\theta_{1,0} = 3.176067131107269$, $\theta_{2,0} = 3.406985767928092$, $\theta_{0,1} = 1.753260803421655$, $\theta_{0,2} = 0.724695975751957$, $\theta_{1,2} = 1.566020932246446$, $\delta_{0,0} = 1.172412555847297$, $\delta_{1,0} = 2.862607698545040$, $\delta_{2,0} = 4.947150771599252$, $\delta_{0,1} = 0.946904335902318$, $\delta_{0,2} = 0.077108238106769$, and $\delta_{1,2} = 1.624416688203425$.

For the numerical continuation computations DSGRN provides sample parameter values from parameter regions and for each sampled parameter point we search for hysteresis using the following procedure.

For ascending (descending) hysteresis we randomly sample 10 initial guesses (x_0^0, x_1^0, x_2^0) satisfying the conditions $0 < x_0^0 \leq \min \theta_{*,0}$, $0 < x_1^0 \leq \min \theta_{*,1}$, and $0 < x_2^0 \leq \min \theta_{*,2}$ ($\max \theta_{*,2} <$

$x_2^0 \leq 2 \max \theta_{*,2}$ for descending hysteresis). For each initial guess (x_0^0, x_1^0, x_2^0) we perform the following computations (where the successive steps are dependent on the successful completion of the previous ones):

1. Run Newton's method with (x_0^0, x_1^0, x_2^0) as initial guess to find an equilibrium solutions to the Hill model with $s = 0$.
2. If Newton's methods converges to an equilibrium solution (x_0, x_1, x_2) check if it satisfies the condition $0 < x_2 \leq \min \theta_{*,2}$ ($\max \theta_{*,2} < x_2$ for descending hysteresis).
3. If the above condition is satisfied we use the solution (x_0, x_1, x_2) and $s = 0$ as the initial point for a pseudo arclength continuation method to compute a curve of equilibria from $s = 0$ up to $s = 4$.
4. During the continuation of the equilibria we identify saddle-node bifurcations by monitoring the sign of the determinant.
5. If during the continuation of the equilibria we get an even number of saddle-node bifurcations and for each bifurcation the value of x_2 just before the bifurcation point is smaller (larger for descending hysteresis) than the value of x_2 just after the bifurcation point, then we declare this a hysteretic curve.

If we get a hysteretic curve for at least one of the random initial guesses we declare the sampled parameter point used for the computations as a *hysteretic parameter point*.

The *hysteresis score* of a set of sampled parameter points is the percentage of hysteretic parameter points in the given set of parameter points. For the computations in Table 1 of the main text and Table S1 we used 1,000 sampled parameter points (1,000 curves) for each of the scores. Networks 33, 108, and 4346 used in Table S1 are shown in Figure S3.

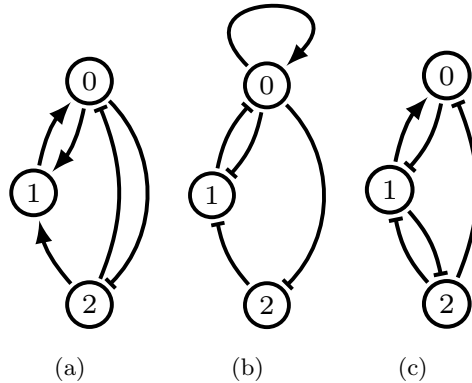


Figure S3: (a) Regulatory network 33. (b) Regulatory network 108. (d) Regulatory network 4346.

C Extending DSGRN capabilities

To be processed by the original DSGRN software [2] a regulatory network was required to satisfy the following conditions:

1. Every node must have an in edge.

2. No repressing self-edges.
3. Every node must have an out edge.

These assumptions are too restrictive as they remove a tremendous number of potentially interesting regulatory networks. The current version of DSGRN [1] overcomes these constraints as indicated below.

C.1 No in edges

As an example consider network 13 or 14 of Figure S2 where node 1 has an out edge, but no in edges. In general if node n has no in-edges the n -th component of (1) reduces to

$$-\gamma_n x_n + \beta$$

and derivation of the parameter regions proceeds as usual (though the computation is trivial) [5].

C.2 Node with a self repressing edge

We begin by quickly surveying how DSGRN produces a state transition graph (STG) that is a representative for the dynamics. For more details see [2]. Consider a regulatory network with N vertices. Let $E(n)$ denote the number of out edges from node n . Thus, the set of threshold values associated with the n -th node is $\Theta(n) := \{\theta_{m_k, n} \mid k = 0, \dots, E(n) - 1\}$ where we assume that $0 < \theta_{m_k, n} < \theta_{m_{k+1}, n}$. The complement of the set of hyperplanes $x_n = \theta_{m_k, n}$, $n = 0, \dots, N - 1$ defines a collection of open cubical subsets of $(0, \infty)^N$. We refer to these sets as *top cells*. We index these cells by $\mathcal{K} := \prod_{n=0}^{N-1} \{0, 1, \dots, E(n)\}$ where (j_0, \dots, j_{N-1}) is the cell containing points x satisfying $\theta_{m_{j_n}, n} < x_n < \theta_{m_{j_n+1}, n}$ with the convention that $\theta_{m_0, n} = 0$ and $\theta_{m_{E(n)+1}, n} = \infty$. The boundaries of the top cells are called *walls* and each *interior* wall, i.e. a wall contained in $(0, \infty)^N$, is a subset of a hyperplane $x_n = \theta_{m_k, n}$. Furthermore, each such wall is the boundary element of exactly two top cells and we use this fact to index the walls by $\mathcal{W} := \{(\kappa_0, \kappa_1)\} \subset \mathcal{K} \times \mathcal{K}$ where the pair (κ_0, κ_1) indicates the wall whose two top cells are indexed by $\kappa_0 = (i_0, \dots, i_{N-1})$ and $\kappa_1 = (j_0, \dots, j_{N-1})$. We refer to i_0, \dots, i_{N-1} as the coordinates of κ_0 . Observe that this allows us to adopt the following convention: the wall indexed by (κ_0, κ_1) is a subset of the hyperplane $x_n = \theta_{m_k, n}$ if and only if $i_n = k - 1$, $j_n = k$, and $i_\ell = j_\ell$ for $\ell \neq n$. If we wish to emphasize this information we write $(\kappa_0, \kappa_1)_{k, n}$. Consider κ_0 and $(\kappa_0, \kappa_1)_{k, n}$. Referring to (1) we define (κ_0, κ_1) to be *repelling* or *absorbing* (in [2] they are referred to as incoming and outgoing, respectively) with respect to κ_0 if

$$-\gamma_n \theta_{m_k, n} + \Lambda_n(x) < 0 \quad \text{or} \quad -\gamma_n \theta_{m_k, n} + \Lambda_n(x) > 0, \quad (2)$$

respectively, for x in the top cell indexed by κ_0 . The opposite set of inequalities are used to define repelling and absorbing with respect to κ_1 .

Observe that the indexing of top cells \mathcal{K} only depends on the ordering of the thresholds, not their numerical values. Thus, \mathcal{K} is a purely combinatorial object. Nevertheless, based on the motivating geometry we say that κ and κ' are *adjacent* if all their coordinate values are the same except for one coordinate and in that coordinate they differ by exactly one. It is only in (2) that the value of the thresholds plays a role. The decomposition of parameter space is chosen such that for each region of the decomposition the inequalities of (2) are preserved.

As is described in [2] if there are no repressive self-edges in the regulatory network, then given (κ_0, κ_1) the options are:

A1 (κ_0, κ_1) is absorbing with respect to κ_0 and repelling with respect to κ_1 ;

A2 (κ_0, κ_1) is repelling with respect to κ_0 and absorbing with respect to κ_1 ;

A3 (κ_0, κ_1) is repelling with respect to both κ_0 and κ_1 .

According to these three options the classical DSGRN defines an edge $\kappa_0 \rightarrow \kappa_1$ in case **A1**, an edge $\kappa_1 \rightarrow \kappa_0$ in case **A2**, and no edge between κ_0 and κ_1 in case **A3** (see Figure S4). We can view this as suggesting that the absorbing direction dictates how one top cell is mapped to a neighboring top cell. Performing this computation over all of \mathcal{W} produces the STG. Observe that \mathcal{K} is the set of vertices of the STG and that edges only exist between adjacent elements of \mathcal{K} .

If there is a repressive self-edge in the regulatory network, then it is possible that (κ_0, κ_1) is absorbing with respect to both κ_0 and κ_1 . The naive response is to introduce edges $\kappa_0 \rightarrow \kappa_1$ and $\kappa_1 \rightarrow \kappa_0$, but this suggests recurrent dynamics where it may not exist. Thus, this case was not considered in the classical DSGRN.

However, based on [2] (see in particular Section 4.2) we claim the results:

R1 Consider (κ_0, κ_1) indexing a wall contained in $x_n = \theta_{n,n}$. Then, $\Lambda_i(x) = \Lambda_i(\bar{x})$ for all $i \neq n$ and for any $x \in \kappa_0$ and $\bar{x} \in \kappa_1$.

R2 In addition, consider (κ'_0, κ'_1) indexing a wall contained in $x_n = \theta_{n,n}$, such that (κ_0, κ'_0) and (κ_1, κ'_1) are indices for walls, i.e. κ_0 and κ'_0 are adjacent as are κ_1 and κ'_1 . If (κ_0, κ'_0) is repelling (absorbing) with respect to κ_0 or κ'_0 , then (κ_1, κ'_1) is repelling (absorbing) with respect to κ_1 or κ'_1 .

We resolve the issue of a self-edge by expanding \mathcal{K} . Fix a region of parameter space. This implies that the inequalities (2) are fixed. Define

$$\mathcal{K}^\perp := \prod_{n=0}^{N-1} \{0, \dots, k, \dots, E^*(n)\}$$

where $E^*(n) = E(n) + 1$ if there is a self-repressing edge to node n and $E^*(n) = E(n)$ otherwise. If there is a self-repressing to node n then the threshold corresponding to this edge is $\theta_{m_k, n}$ with $m_k = n$ and we indicate this by denoting $k_-^* = k$ and $k_+^* := k + 1$. In this case it is possible to have a wall $(\kappa_0, \kappa_1)_{k, n}$ such that (κ_0, κ_1) is absorbing with respect to both κ_0 and κ_1 . Again based on [2] this is only possible for the k corresponding to the k_\pm^* above. To define the STG we need to consider adjacent cells in \mathcal{K}^\perp , i.e., the set $\mathcal{W}^\perp := \{(\kappa_0, \kappa_1)\} \subset \mathcal{K}^\perp \times \mathcal{K}^\perp$ where again it is assumed that a single coordinate of κ_1 is larger than the coordinate in κ_0 . Let $(\kappa_0, \kappa_1) \in \mathcal{W}^\perp$. If neither κ_0 nor κ_1 contain a k_\pm^* as a coordinate, then we use the classical DSGRN rules based on **A1** - **A3**. Thus, we only need to consider $(\kappa_0, \kappa_1) \in \mathcal{W}^\perp$ where either κ_0 or κ_1 contains k_\pm^* as a coordinate. Consider $(\kappa_0, \kappa_1)_{k_-^*, n}$. Then the classical DSGRN rules apply to determine whether (κ_0, κ_1) is absorbing or repelling with respect to κ_0 . If (κ_0, κ_1) is absorbing (repelling) with respect to κ_0 , define (κ_0, κ_1) is repelling (absorbing) with respect to κ_1 . Consider $(\kappa_0, \kappa_1)_{k_+^*, n}$. Then the classical DSGRN rules apply to determine whether (κ_0, κ_1) is absorbing or repelling with respect to κ_1 . If (κ_0, κ_1) is absorbing (repelling) with respect to κ_1 , define (κ_0, κ_1) is repelling (absorbing) with respect to κ_0 . Now assume that a k_\pm^* is a coordinate of both κ_0 and κ_1 and hence we need to consider $(\kappa_0, \kappa_1)_{\ell, n'}$. Once again there are three cases to consider $\ell = k_-^*$, $\ell = k_+^*$, or the ℓ -th threshold is not associated with a repressive self-edge. Classical DSGRN does not apply for determining absorbing and repelling in any of these cases. To determine this consider $\kappa_0^\pm, \kappa_1^\pm \in \mathcal{K}^\perp$ such that (see Figure S4)

$$(\kappa_0^-, \kappa_1^-), (\kappa_0^+, \kappa_1^+), (\kappa_0^-, \kappa_0), (\kappa_0, \kappa_0^+), (\kappa_1^-, \kappa_1), (\kappa_1, \kappa_1^+) \in \mathcal{W}^\perp.$$

Note that while κ_0^\pm or κ_1^\pm must exist, it is possible that only one pair exists. Also observe that classical DSGRN applies to the pairs κ_0^\pm and κ_1^\pm and thus absorbing and repelling of (κ_0^-, κ_1^-) and (κ_0^+, κ_1^+) is determined. If both κ_0^\pm and κ_1^\pm exist, then by **R2** (κ_0^-, κ_1^-) is absorbing/repelling with respect to κ_0^- (κ_1^-) if and only if (κ_0^+, κ_1^+) is absorbing/repelling with respect to κ_0^+ (κ_1^+). We define (κ_0, κ_1) to be absorbing/repelling with respect to κ_0 (κ_1) in accordance with (κ_0^-, κ_1^-) or (κ_0^+, κ_1^+) .

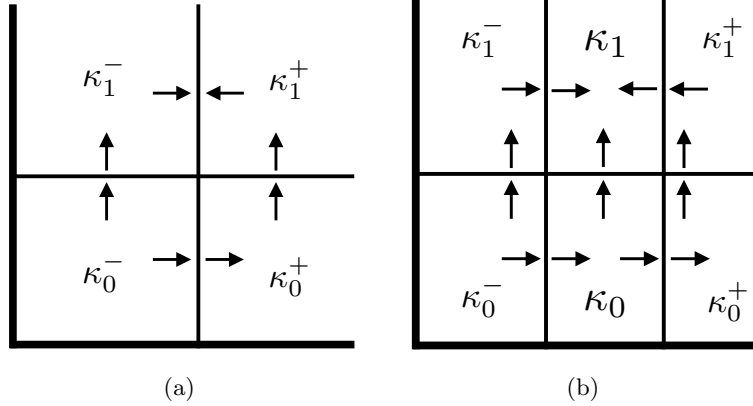


Figure S4: (a) A potential original DSGRN complex \mathcal{K} where the vertical threshold is associated with a self-repressing edge. An arrow going from a top cell κ_i to a wall indicates an absorbing wall and an arrow from a wall to a top cell indicate a repelling wall. (b) Portion of the refined DSGRN complex \mathcal{K}^\dagger . The cells κ_0 and κ_1 are the additional cells in the refined complex. The wall labelling in (b) induces the edges $\kappa_0^- \rightarrow \kappa_0$, $\kappa_0^- \rightarrow \kappa_1^-$, $\kappa_0 \rightarrow \kappa_0^+$, $\kappa_0 \rightarrow \kappa_1$, $\kappa_1^- \rightarrow \kappa_1$, and $\kappa_1^+ \rightarrow \kappa_1$ in the STG on \mathcal{K}^\dagger .

C.3 Node without an out-edge

DSGRN uses the thresholds corresponding to the out-edges of each node to construct the cubical complex \mathcal{X} decomposing the phase space. For this reason the original DSGRN does not allow for nodes in the network without at least one out-edge [2]. We address this limitation in the following way. We treat a node without out-edges as if it had one single out-edge. In particular, we use the parameter factor graph of a node with a single out edge in the construction of the parameter graph for this node. Hence if x_i is a node without an out-edge, in the parameter decomposition for this node there is a threshold $\theta_{\emptyset,i}$ that is not associated to any edge in the network. Using this approach we have at least one threshold for every node and can construct the cubical complex \mathcal{X} as it is done in the original DSGRN. The threshold $\theta_{\emptyset,i}$ is only used to determine the cubical complex \mathcal{X} at the node x_i and it does not affect the other nodes of the network. In the DSGRN output of parameter inequalities this threshold is displayed as $T[x_i \rightarrow]$.

References

- [1] Shaun Harker Bree Cummins, Marcio Gameiro. DSGRN: Dynamic Signatures Generated by Regulatory Networks. <https://github.com/marciogameiro/DSGRN>, 2020.
- [2] Bree Cummins, Tomas Gedeon, Shaun Harker, Konstantin Mischaikow, and Kafung Mok. Combinatorial representation of parameter space for switching networks. *SIAM Journal on Applied Dynamical Systems*, 15(4):2176–2212, 2016.

- [3] Timothy Gardner, Charles Cantor, and James Collins. Construction of a genetic toggle switch in *Escherichia coli*. *Nature*, 403(6767):339–342, 2000.
- [4] H. B. Keller. *Lectures on numerical methods in bifurcation problems*, volume 79 of *Tata Institute of Fundamental Research Lectures on Mathematics and Physics*. Springer-Verlag, Berlin, 1987.
- [5] Shane Kepley, Konstantin Mischaikow, and Lun Zhang. Computing linear extensions for boolean lattices with algebraic constraints. <https://arxiv.org/abs/2006.02622>, 2020.